Earth and Planetary Science Letters 361 (2013) 229–237

Contents lists available at SciVerse ScienceDirect

Earth and Planetary Science Letters

journal homepage: www.elsevier.com/locate/epsl

Experimental low-grade alteration of biogenic magnetite indicates microbial involvement in generation of banded iron formations

Yi-Liang Li [a,*], Kurt O. Konhauser [b], Andreas Kappler [c], Xi-Luo Hao [a]

[a] Department of Earth Sciences, the University of Hong Kong, Hong Kong
[b] Department of Earth and Atmospheric Sciences, the University of Alberta, Edmonton, Alberta, Canada T6G 2E3
[c] Geomicrobiology, Center for Applied Geosciences, University of Tübingen, Sigwartstrasse 10, D-72076 Tübingen, Germany

ARTICLE INFO

Article history:
Received 24 May 2012
Received in revised form
18 October 2012
Accepted 27 October 2012
Editor: G. Henderson
Available online 30 November 2012

Keywords:
Precambrian
banded iron formation
dissimilatory iron-reducing bacteria
biogenetic magnetite
photosynthesis
electron microscope

ABSTRACT

During the deposition of banded iron formation (BIF), the downward flux of ferric oxyhydroxides and phytoplankton biomass should have facilitated Fe(III) reduction during burial, with the end product being ferrous iron-containing minerals including magnetite. Although earlier studies have attempted to quantify the significance of this pathway based on models of the ancient Fe cycle, the only direct evidences of a biological role in magnetite formation in BIF are their iron isotope compositions and unique crystallography which are reminiscent of biologically-generated magnetite. However, the biogenesis hypothesis lacks an explanation as to why modern biogenic magnetite crystals are generally a few hundred nm or smaller in size, yet the magnetite crystals in BIF are mostly tens of micrometers or larger in size. In this study, we demonstrate that biogenic magnetite crystals can grow in size upon reaction between oxyhydroxide and microbial biomass after compression and heating to 1 kbar and 150 °C, respectively. The magnetite crystals previously produced by *Thermoanaerobacter spp.* TOR39 reach sizes in excess of 700 nm after the P–T experiments, while new magnetite grains >400 nm formed from the superparamagnetic magnetite-dominated end product of *Shewanella* sp. culture. This study indicates that the large magnetite crystals observed in BIF can be derived through a three-stage sequence, beginning with dissimilatory iron reduction of an initial ferric iron-rich sediment coupled to the oxidation of dead phytoplankton biomass, followed by magnetite crystal aging, and ultimately pressure–temperature induced abiotic alteration of the biogenic magnetite during metamorphism.

1. Introduction

Banded iron formations (BIFs) are characterized by their alternating iron-rich and silica-rich layers that were precipitated throughout much of the Late Archean and Paleoproterozoic (2.7–1.9 Ga) (Klein, 2005; Bekker et al., 2010). The main mineralogy of the least metamorphosed BIF consists of chert (SiO_2), magnetite (Fe_3O_4), hematite (Fe_2O_3), siderite ($FeCO_3$) and various iron–silicate minerals, such as greenalite ($(Fe)_3Si_2O_5(OH)_4$); the presence of both ferric and ferrous minerals gives BIF an average oxidation state of $Fe^{2.4+}$ (Klein and Beukes, 1992). It is generally agreed that none of the minerals in BIF are primary, but that instead, the minerals reflect both diagenetic and metamorphic overprinting. For instance, the primary ferric iron minerals were most likely ferric oxyhydroxides, such as ferrihydrite [$Fe(OH)_3$] (Klein, 2005; Bekker et al., 2010).

The mineralogy of BIF dictates that some oxidation of dissolved Fe(II) was necessary for the formation. Two biological models have been proposed that involve the metabolic activity of planktonic bacteria in the oceans' euphotic zone. Perhaps in the more ancient mechanism, primitive anoxygenic photosynthetic bacteria may have used dissolved Fe(II) as a reductant for CO_2 fixation, producing dissolved Fe(III) which then immediately hydrolyzed to a ferric oxyhydroxide mineral by-product (Hartman, 1984). A number of purple and green phototrophic bacteria exist today that utilize this metabolism (Hegler et al., 2008), and given their highly efficient light harvesting mechanisms, they may have been able to grow to depths greater than 100 m in the water column (Kappler et al., 2005). Modeling of experimentally determined photosynthetic Fe(II) oxidation rates even suggests that such microorganisms could have accounted for all of the Fe(III) initially deposited in primary BIF sediment (Konhauser et al., 2002). Chemical oxidation of Fe(II) by photosynthetically produced O_2 is a second possibility, allowing for the indirect biogenic precipitation of ferric oxyhydroxides. Under an anoxic atmosphere, this O_2 could have been confined to localized "oxygen oases" associated with cyanobacterial blooms in coastal settings (Cloud, 1965, 1973). Cloud (1965, 1973) further proposed that such primitive O_2-producing photosynthetic bacteria, which

* Corresponding author. Tel.: +852 28598021; fax: +852 25176912.
E-mail address: yiliang@hku.hk (Y.-L. Li).

0012-821X/$ - see front matter © 2012 Elsevier B.V. All rights reserved.
http://dx.doi.org/10.1016/j.epsl.2012.10.025

lacked suitably advanced oxygen-mediating enzymes, required ferrous iron to detoxify oxygen. If so, these microorganisms would have flourished specifically when Fe(II) and nutrients were made episodically available (Fralick and Pufahl, 2006). Once oxygen was present, microaerophilic Fe(II) oxidizers could have contributed to the direct precipitation of ferric oxyhydroxide minerals (Holm, 1989).

If a biological mechanism was important in the initial process of Fe(II) oxidation in the Archean euphotic zone, it is then expected that biomass settled to the seafloor along with the ferric oxyhydroxide minerals (Posth et al., 2010; Konhauser et al., 2011). Yet, BIFs contain very little organic carbon, meaning that the biomass was oxidized either by the combined metabolic processes of fermentation and chemoheterotrophy during diagenesis (Konhauser et al., 2005) or abiotically at higher temperatures associated with metamorphism (Dimroth, 1976). Coupling the reduction of Fe(III) minerals to the oxidation of organic matter not only explains the low content of organic carbon in BIF via the consumption of carbon (BIFs have on average <0.5 wt% organic carbon; Gole and Klein, 1981), but it also explains the textural features in the reduced iron minerals in BIF, such as magnetite. For instance, the presence of magnetite as (1) disseminated grains within but obscuring sedimentary laminae, (2) laminated beds that clearly truncate sedimentary layering, and (3) cleavage fills, imply a secondary origin to this magnetite (Krapež et al., 2003). Ewers and Morris (1981) even suggested that in the 2.48 Gyr old Dales Gorge Formation of Western Australia, most magnetite in the BIF was secondary, having overgrown a fine-grained ferric iron oxide precursor.

Four lines of evidence support the notion that magnetite formation during diagenesis was initially driven by dissimilatory ferric-iron reduction (DIR), a form of chemoheterotrophic metabolism used by bacteria (reaction 1); the Fe^{2+} that is produced by this metabolism adsorbs onto other ferric oxyhydroxide grains, where through solid-state conversion it ultimately crystallizes to magnetite (reaction 2).

$$CH_3COO^- + 8Fe(OH)_3 \rightarrow 8Fe^{2+} + 2HCO_3^- + 15OH^- + 5H_2O \quad (1)$$

$$2OH^- + Fe^{2+} + 2Fe(OH)_3 \rightarrow Fe_3O_4 + 4H_2O \quad (2)$$

First, extant hyperthermophilic *Bacteria* and *Archaea* branch deeply in the universal phylogenetic tree (i.e., they represent an ancient metabolism) can reduce Fe(III) (Vargas et al., 1998). Second, highly negative δ^{56}Fe values in magnetite-rich BIF samples as old as 2.9 Ga have been observed (Johnson et al., 2003; Yamaguchi et al., 2005) and are comparable to the negative fractionations measured in experimental culture with dissimilatory Fe(III)-reducing bacteria (e.g., Johnson et al., 2005). Third, Li et al. (2011a) conducted high resolution magnetite analyses on the 2.48 Gyr old Dales Gorge Member BIF and reported magnetite with a lattice constant and Fe^{2+}/Fe^{3+} stoichiometry very similar to those produced by DIR bacteria, *Geobacter*, *Shewanella* and *Thermoanaerobacter*. Fourth, biogenic magnetite crystals have very pure chemical compositions, which is regarded as one of the major criteria for assigning a biogenic origin to magnetite (e.g., Chang and Kirschvink, 1989; Thomas-Keprta et al., 2000; Bazylinski et al., 2007). Magnetite in BIF can also have a pure end-member composition (e.g., Klein, 1974; Gole, 1981).

Naturally, an abiotic mechanism is also possible, and is likely upon burial temperatures in excess of those permitting microbial life. Indeed, the respiration of ferric oxyhydroxides by DIR bacteria has been documented to be able to produce magnetite from subzero temperatures to as high as 103 °C (Kashefi and Lovley, 2003). By contrast, the previously reported lowest temperature needed for the abiotic reaction between simple organic compounds and ferric iron (i.e., reaction 1) is at least 250 °C (Viswanathiah et al., 1980). The decomposition of siderite can also lead to magnetite formation at high metamorphic temperature (reaction 3) (e.g., Ayres. 1972; Kaufman, 1996; Thomas-Keprta et al., 2009).

$$3FeCO_3 + H_2O \rightarrow Fe_3O_4 + 3CO_2 + H_2 \quad (3)$$

Despite the plausibility of magnetite formation being linked to the oxidation of planktonic biomass, there has been a long-standing issue as to why the magnetite precipitated in modern environments and experimental studies differs in terms of size and texture from the magnetite in BIF. In contrast to the μm or larger size magnetite crystals in BIF (e.g., La Berge, 1964; Floran and Papike, 1975; Ewers and Morris, 1981; Koehler et al., 2010), the so far reported biogenic extracellular magnetite crystals are mostly superparamagnetic and dominated by ultrafine crystals only a few nm to a few hundred nm in size (Sparks et al., 1990; Hanzlik et al., 1996; Roh et al., 2003; Li et al., 2009). At relatively high growth temperatures, as would be expected with sediment burial (>70 °C), the thermophilic bacteria *Theromanaerobacter spp*. can facilitate the production of magnetite of >130 nm (Liu et al., 1997; Zhang et al., 1998), but this is still ~40 times smaller than the smallest single crystals (~5 μm) in BIF ever reported (French, 1968). Moreover, DIR induced magnetite particles have poor crystallinity and irregular morphology (Sparks et al., 1990; Frankel and Bazylinski, 2003) compared to the euhedral magnetite typical of BIF (Gole, 1980; Krapež et al., 2003; Frost et al., 2007; Koehler et al., 2010). These differences need to be reconciled before a biological origin of magnetite in BIF can be more widely accepted. In this regard, we report here how low-grade metamorphic conditions can alter DIR magnetite crystals to those identical in BIF.

2. Samples and experiments

The BIF core samples were from the 2460 Myr old (Pickard, 2003) Kuruman BIF of Transvaal Group in the Northern Cape Province, South Africa. These rocks experienced metamorphic conditions equivalent to burial at 170 °C and 1.2 kbar (e.g., Miyano and Klein, 1983). Thin sections of the BIF were prepared and polished to get a surface roughness near ~200 nm. The edges were subsequently scrapped with an ethanol-cleaned screwdriver to peel off thin flakes to produce conchoidal, concave surfaces for immediate and direct observation under the scanning electron microscope (SEM) to prevent any contamination. The cm-scaled specimens were analyzed using backscatter electron (BSE) mode on a Hitachi S3400 SEM for mineral compositions with contrasting electron densities. Hitachi S4800 FEG SEM was used in secondary electron (SE) mode at low voltages (3–5 kV) and high voltages (20 kV) for imaging of high resolutions. The in situ chemical compositions of the magnetite crystals were measured by equipped energy dispersive X-ray spectroscopy (EDS) at 20 kV. A Philips Tecnai G2 20 S-TWIN scanning transmission electron microscope (STEM) equipped with selected area electron diffraction (SAED) was used for the high resolution observation of mineral morphology and crystallographic structures.

Thermoanaerobacter spp. strain TOR39 and *Shewanella putrefaciens* strain CN32 were grown under strict anoxic conditions with medium revised from Roh et al. (2003). Bicarbonate was omitted to avoid precipitation of Fe(II)-carbonate; a few drops of phosphate stock solution (K_2HPO_4, 0.2 M) were injected to the media before inoculations to get a final concentration of ~2 μM to avoid precipitation of Fe(II)-phosphate and to prevent a negative influence of the phosphate on crystal growth during P–T-treatments. Two-line ferrihydrite ($Fe_5^{3+}HO_8 \cdot 4H_2O$), synthesized according to Cornell and Schwertmann (1996), was supplied as the electron acceptor for both CN32 and TOR39. CN32 was grown with lactate as the carbon source at 30 °C, while TOR39 was grown at 55 °C with

glucose as the carbon source. The metabolism of CN32 leads to the mineralization of magnetite after ~20 h of incubation while that of TOR39 required 7 days. Some TOR39 tubes were further incubated at 55 °C without disturbance for more than two years. The mineral precipitates in tubes of TOR39 and CN32 were extracted by applying a permanent magnet and washed briefly with anhydrous methanol, and dried in the anoxic chamber.

For the high P–T treatment, samples were loaded into Au-tubes and sealed under a flux of argon gas, and then brought to 150 °C and 1 kbar for a week. Different from the TOR39-magnetite product, the CN32-magnetite was previously added to a tiny amount of methyl esters of fatty acids with C8-C24 for the other experiments, which did not influence the experimental results of this study at all. The TOR39- and CN32-magnetite materials before and after the high P–T-treatments were examined by the above-mentioned SEM and STEM methods.

3. Results

3.1. Magnetite in banded iron formations

The Kuruman BIF is characterized by microbanding in the order of <1 mm, and consists of layers of magnetite and chert (Fig. 1A and B). The BSE mode SEM observations revealed that magnetite-rich bands have individual magnetite crystals ranging from a few μm to >110 μm in diameter, with an average of 33 ± 27 μm (Fig. 1B). We commonly observed that small magnetite crystals of only a few μm coexist with larger crystals in the magnetite bands (Fig. 1C). In particular, Fig. 1D is a magnetite crystal 2.2 μm in diameter, as observed in BSE mode. Magnetite appeared sporadically in hematite-rich bands (Fig. 1E and F), with sizes similar to those in the magnetite-rich bands (Fig. 1A and B). The smallest magnetite observed in the Kuruman BIF was approximately 2.2 μm (Fig. 1D and Fig. 1E and F arrowed), which was similar to the previously observed "primary" magnetite of ~5 μm in Biwabik Formation (French, 1968; Frost et al., 2007). Despite the wide distribution of BIF magnetite crystal sizes, all consist of euhedral octahedrons, and they did not show any reaction textures as might be expected from post-depositional interactions with co-existing minerals. These observations suggest a competitive growth history of magnetite crystals, starting with much smaller "crystal seeds" and then increasing in size during crystal growth. Accordingly, it should be possible to experimentally test whether nanometer-sized biogenic magnetite crystals can be enlarged during the post-depositional processes. For this purpose, magnetites produced in the cultures of CN32 and TOR39 were chosen for the high P–T-treatments.

3.2. Biogenic magnetite crystals before and after high T–P treatments

STEM analyses showed that strain CN32 produced ultrafine magnetite particles making highly aggregated clusters (Fig. 2A and B) with

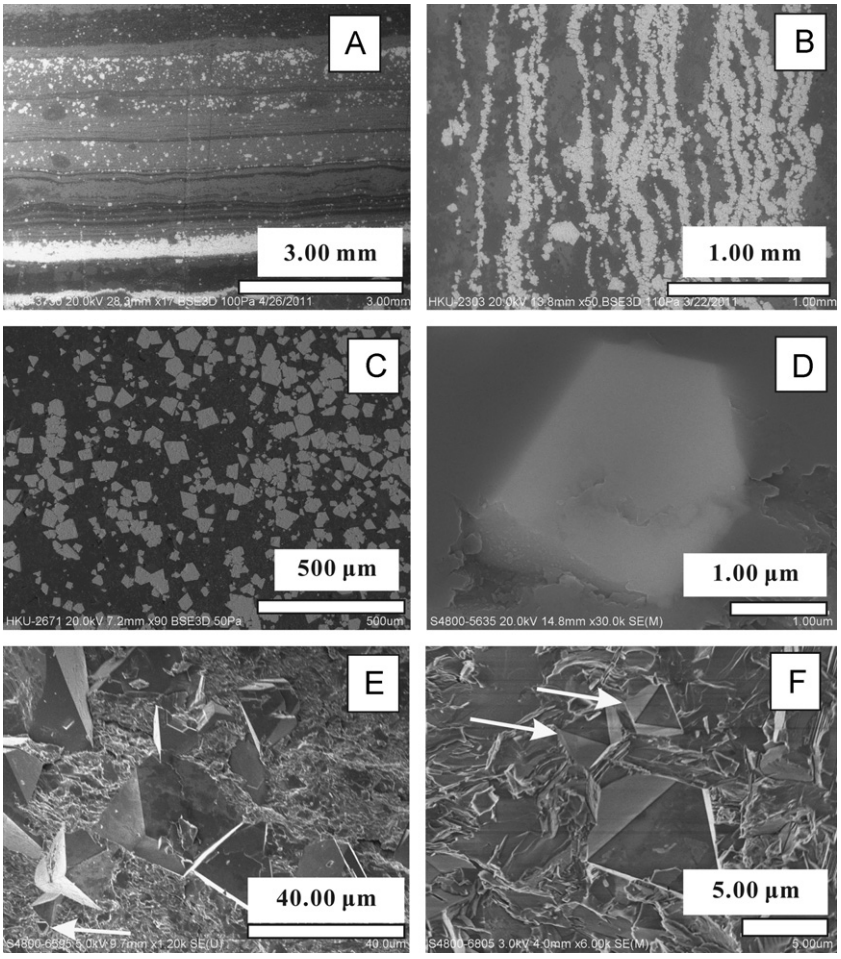

Fig. 1. A section of BIF from the Kuruman Formation, South Africa. (A) Magnetite band and magnetite-rich bands. (B) The thinnest magnetite bands made of magnetite single crystals. (C) The BSE mode of SEM observation shows the scattered magnetite of a few μm to >60 μm in the matrix of chert. (D) A small magnetite crystal of 2.2 μm. (E)–(F) SE mode of SEM images of ~2.2 μm magnetite (arrowed) coexisting with crystals of >30 μm.

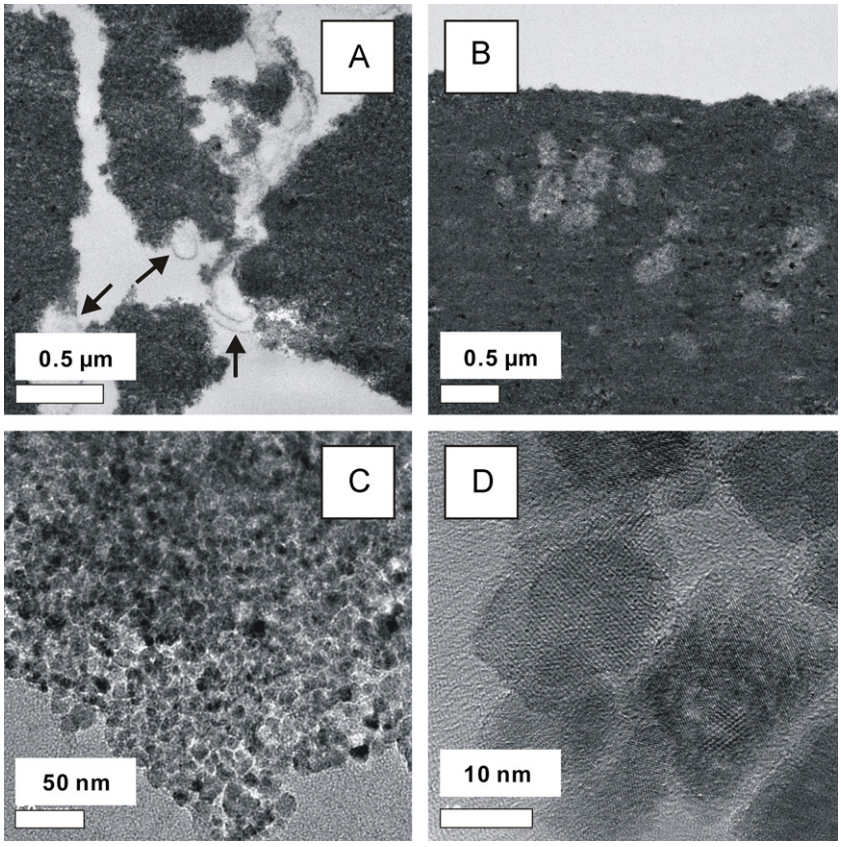

Fig. 2. Magnetite from the culture of *S. putrefaciens* CN32 before the high P–T treatment characterized by STEM. (A) Cell remains (arrowed) mixed with magnetite aggregates. (B) Aggregates of extremely fine-grained magnetite. (C)–(D) High resolution observations which indicated the crystals are around 11 nm.

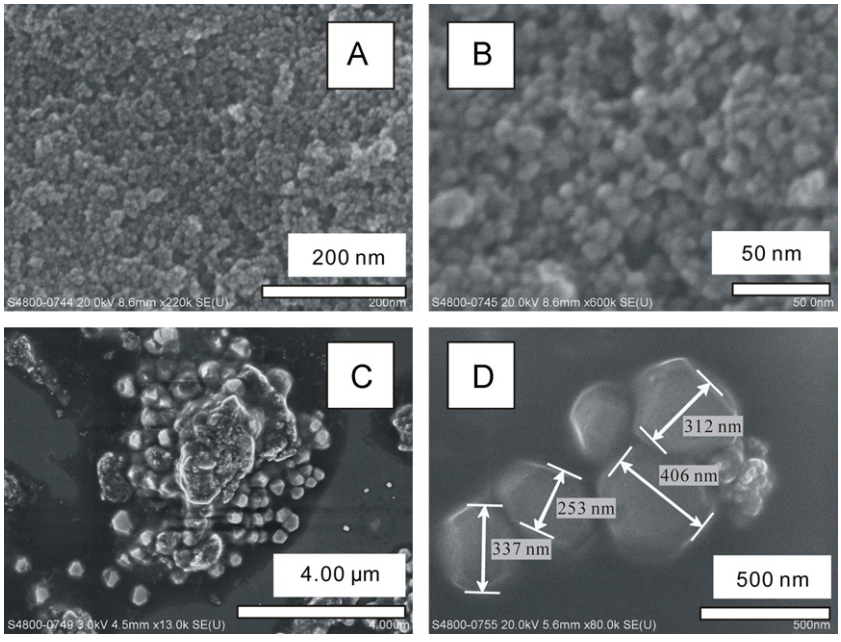

Fig. 3. Magnetite from the culture of *S. putrefaciens* CN32 after the high P–T treatment characterized by SEM. (A)–(B) Single particles can be recognized under high resolutions. (C) Aggregates of magnetite of much big size coexisting with original fine particles. (D) A few big magnetite crystals with measured sizes.

individual sizes in the order of 10 s of nanometers in diameter (Fig. 2C and D). The images at high resolution (Fig. 2C and D) are similar to those previously reported for magnetite crystals produced by *Shewanella* (Hanzlik et al., 1996; Li et al., 2009).

After the high P–T treatment, the major fraction of magnetite particles remained in the ultrafine size range (Fig. 3A and B), while there was a small fraction of newly nucleated magnetite crystals with crystal sizes significantly greater than those prior to the metamorphic conditions (Fig. 3C and D). The magnetite in Fig. 3C appeared to be "dirty" as it shows electronic charging features likely resulting from the crystals having been coated by remains of organic material even after the high P–T treatment.

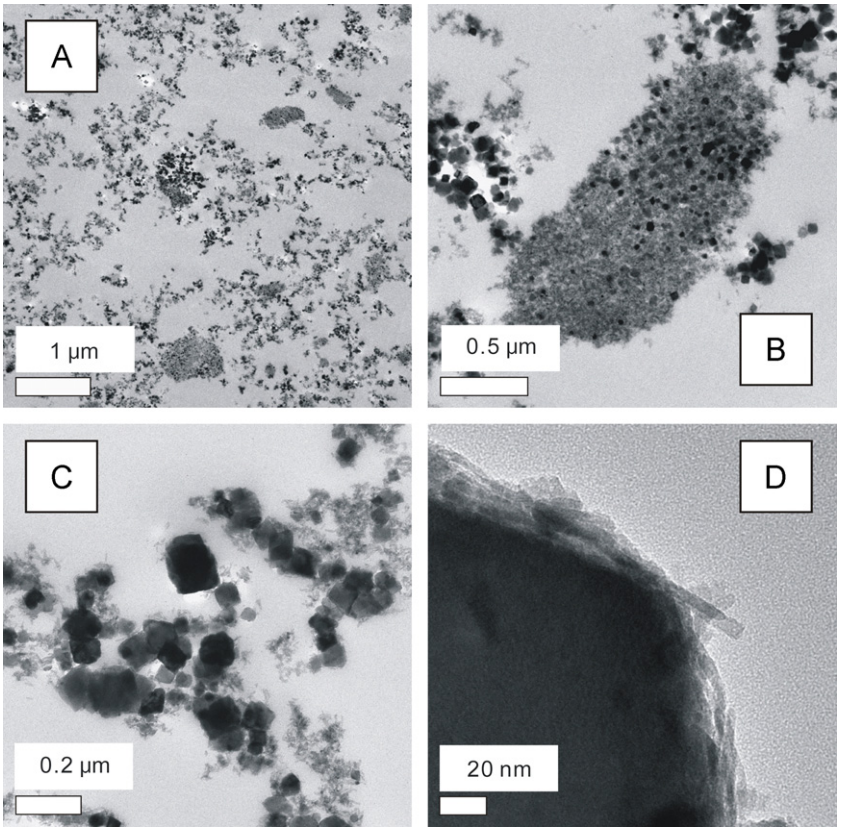

Fig. 4. STEM characterization of magnetite produced by *Thermoanaerobacter spp.* TOR39 at 55 °C before the high P–T treatment. (A)–(B) Scattered magnetite crystals and those aggregated by cell remains. (C) Fine oxyhydroxide particles on the surface of magnetite crystal. (D) Ultrafine goethite needles absorbed on a magnetite crystal.

Most of the larger magnetite particles had sizes around 255 ± 65 nm, although some larger crystals reached > 400 nm in diameter (Fig. 3D).

The TOR39-magnetite was characterized by STEM before the high P–T treatment. Magnetite crystals were either scattered or aggregated by the cellular remains (Fig. 4A and B). The remains of ferrihydrite could easily be observed along with magnetite crystals (Fig. 4C), while the formation of secondary Fe(III)-oxyhydroxide (goethite) was evident on the surface of magnetite crystal at high resolution (Fig. 4D). The absorption of organic matter on magnetite (i.e., cellular remains), however, was best viewed under low voltage (3–5 kV) SE mode SEM imaging because the secondary electrons of low voltage carry more surface information. Fig. 5A highlights the coexistence of cellular remains and magnetite. Large magnetite aggregates rich in organic matter were made by the mixing of magnetite and organic matter (Fig. 5B and C). After high P–T treatment, some magnetite crystals substantially increased their sizes (Fig. 6). For instance, Fig. 6A shows a loose stack of magnetite crystals without organic remains, while Fig. 6B–D displays magnetite crystals with a wide distribution of sizes, some > 700 nm (Fig. 6D).

As both the nucleation of new crystals in CN32-magnetite or the increased crystal size of TOR39-magnetite were likely to be surficial processes, the surface of magnetite crystals from BIF and those from the microbial incubations were compared. Both the rims of BIF- and TOR39-magnetite crystals show the existence of a corona of amorphous iron (Fig. 7). The amorphous corona of the BIF-magnetite was around 10 nm (Fig. 7A), while that of the biogenic magnetite after the high P–T treatment was ~20 nm (Fig. 5B). Some parts of the corona of BIF magnetite showed lattice fringes that indicate only localized ordered-structures. By contrast, the superparamagnetic magnetite from the CN32 culture did not show a corona of amorphous ferric iron before or after the high P–T treatment due to the ultrafine particle size.

4. Discussion

The crystal size of TOR39-magnetite experienced three stages of development: (1) the initial nucleation and growth of nanometer-sized crystals due to DIR, (2) further growth and aging during prolonged incubation, and (3) crystal enlargement to submicrometer sizes under conditions similar to low-grade metamorphism. The TOR39 mediated nucleation of magnetite is the first stage, during which the nucleation and growth of crystals is constrained by the kinetics of the enzymatic reduction of Fe(III), including changes in cell density (Zegeye et al., 2010), the concentration of the water-soluble Fe(III) and Fe(II) (e.g., Li et al., 2011b), and the amount of ferrihydrite present (Piepenbrock et al., 2011). After cell lysis, the ongoing growth of crystals during the second stage is facilitated by the existence of high concentrations of soluble Fe(II) and Fe(III) (Li et al., 2011b), and the surplus ferrihydrite (e.g., Li et al., 2009). Zhang et al. (1998) previously reported the nucleation of magnetite of < 10 nm after only 10 h incubation with TOR39; these grew to ~130 nm after 528 h of incubation at 65 °C. In this study, the magnetite crystals from the TOR39 culture after 7 days of incubation at 55 °C were on average 91 ± 44 nm in diameter (Fig. 4B and C); magnetite from the same culture further incubated for over two years reached sizes of 360 ± 46 nm on average (Fig. 5C). The third stage is the high P–T treatment that promoted progressive enlargement of the crystals by new overgrowth on the magnetite surfaces. The TOR39 cultures dried and treated at 150 °C and 1 kbar for 7 days have crystal sizes averaging 565 ± 107 nm in diameter (Fig. 6), while the > 700 μm magnetite

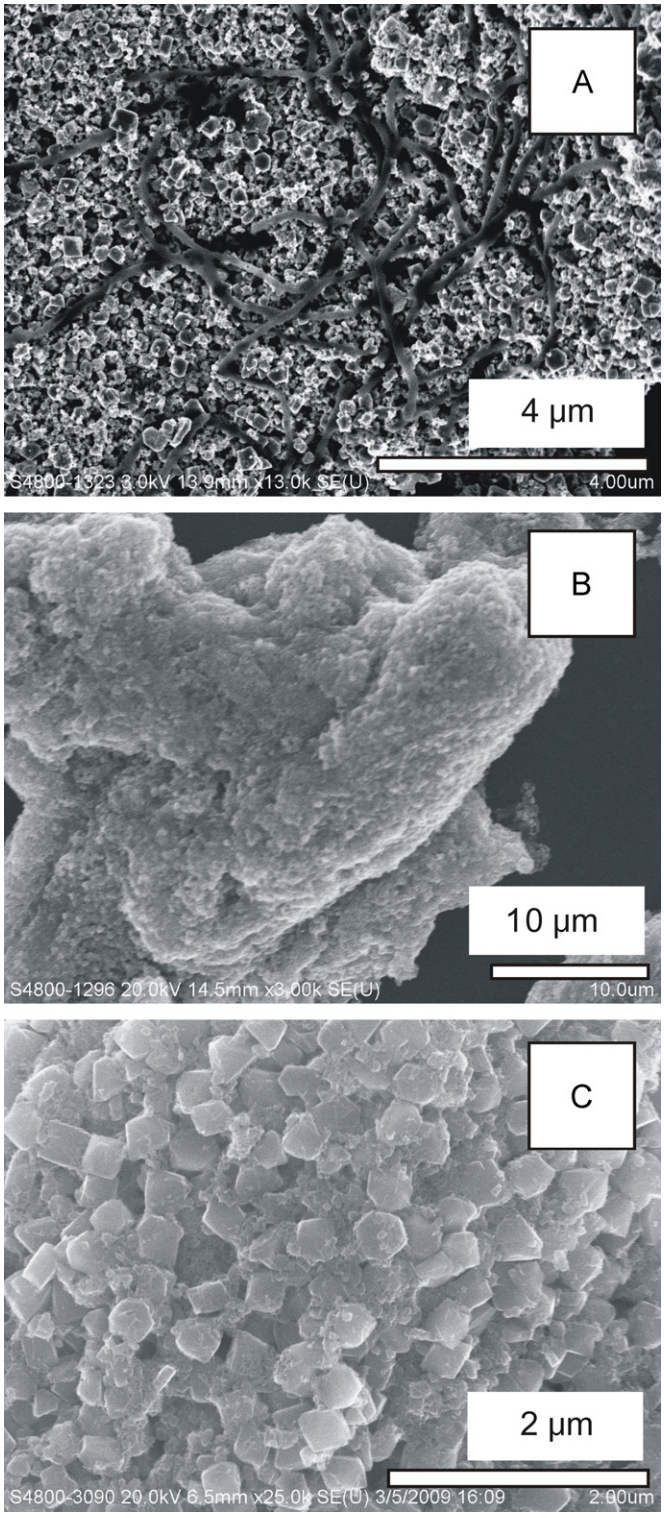

Fig. 5. TOR39-magnetite before the high P–T treatment observed by SEM. (A) Cell remains coexisting with magnetite. (B) Magnetite aggregated by rich organic matter. (C) Amplification of the local of B showing stacked magnetite crystals.

produced in the high P–T experiment was close to the smallest euhedral magnetite observed in BIF (Fig. 1D–F; French, 1968; Frost et al., 2007). Collectively, these three stages could be considered corresponding to the (1) biogenic, (2) consolidation or early diagenetic, and (3) the low-grade metamorphic stages experienced by magnetite during BIF sediment burial.

In the TOR39 cultures, although all magnetite crystals were associated with the ferrihydrite precursor and surrounded by organic materials, only a small fraction of magnetite crystals actually accreted. The widening of size distribution and shift of the average crystal size of magnetite by this high P–T treatment resulted in large euhedral magnetite grains and clusters of small magnetite grains, similar to magnetite in BIF (Fig. 1C; Klein and Fink, 1976). This phenomenon can be explained by the Ostwald ripening process (e.g., Kallay and Žalac, 2002) in which the competitive growth of particles occurred within limited volume at high P–T conditions. In the CN32 culture, the nucleation of new magnetite crystals from the highly aggregated nanoparticle of magnetite ($\sim$11 nm, Fig. 2C and D) likely occurred via the high P–T enhanced contacting of the surface diffusion layer of particles through competitive growth (Marqusee and Ross, 1984).

The observation that organic carbon co-precipitated with magnetite in the DIR cultures (Li et al., 2011a; Perez-Gonzalez et al., 2010; this study) provides a scenario similar to the previous studies on the incorporation of trace amount of organics in BIF (Posth et al., 2008; Li et al., 2011a). The incomplete reduction of ferric oxyhydroxides through DIR can result in magnetite-rich sediments containing residual amounts of organics (e.g., Fredrickson et al., 1998; Li et al., 2009). During the diagenetic or early metamorphic stages, the sediment pore fluids could bring Fe(II) to the organic materials and Fe(III) already absorbed by magnetite for the further growth of magnetite crystals. With organics and primary ferrihydrite proximal to the surface of magnetite (Fig. 4B–D, Fig. 5), the high P–T treatment (reaction 2) facilitated the transformation of the corona of amorphous ferric iron to magnetite and thus the accretion of the existing magnetite crystals.

Although the decomposition of siderite at metamorphic conditions may also produce magnetite (e.g., Kaufman, 1996), those crystals tend to be single-domain magnetite with sizes <200 nm, even at higher temperatures (550 °C, Golden et al., 2004). The hydrothermal synthesis of magnetite at elevated temperatures may produce magnetite with a narrow distribution of crystal sizes owing to the homogeneous reaction system (Viswanathiah et al., 1980), which is different from either the size distribution of BIF magnetite (Fig. 1C; Pecoits et al., 2009) or the size distribution of biogenic magnetite after the high P–T-treatments (this study). The accretion of the TOR39-magnetite can also explain the previous observations of Fe isotopic zonations in single crystals of BIF-magnetite. In magnetite of BIF from Old Wanderer, Zimbabwe, the δ^{56}Fe of the core of crystal was found lighter than that of the rim (Steinhoefel et al., 2009), indicating a dynamic growth of crystals that resulted in a Rayleigh fractionation of Fe isotopes in a relatively enclosed system (e.g., Frost et al., 2007; Johnson et al., 2005). As this process may produce a significant amount of water (reaction 2), an external fluid source for the activation of the mineral recrystallization, which leads to Fe isotopic fractionation, is not necessary when the sediment becomes subjected to low grade metamorphism.

Several recent studies have suggested that photoautotrophic bacteria flourished in the euphotic zone of the Archean–Palaeoproterozoic oceans (e.g., Nesbit and Sleep, 2001; Konhauser et al., 2002; Kappler et al., 2005; Blank and Sánchez-Baracaldo, 2010). Similarly, cellular remains have been widely observed to co-precipitate with the amorphous ferric iron particles in the modern euphotic zone (Banfield et al., 2000). Schädler et al. (2009) also experimentally demonstrated that phototrophic Fe(II)-oxidizers could produce ferric oxyhydroxide–cell biomass aggregates, that in the ocean, would have led to their precipitation to the seafloor. The juxtaposition of an electron donor (cells) and electron acceptor (ferric iron) would then have facilitated DIR during diagenesis, and whatever organic carbon was not respired,

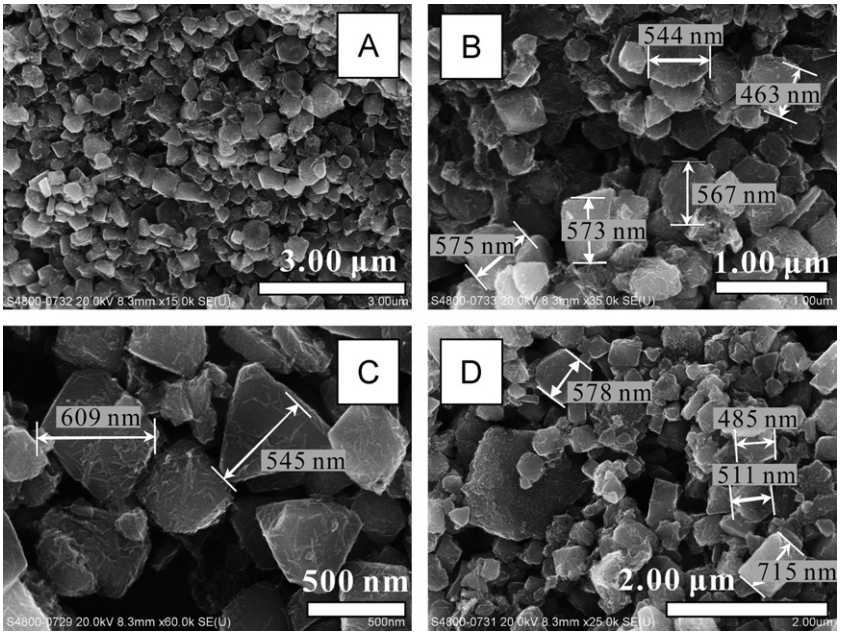

Fig. 6. TOR39-magnetite after the high P–T treatment observed by SEM. (A) Magnetite loosely stacked. (B)–(D) Large magnetite crystals with their measured sizes. Note the needle-like goethite adsorbed on the surface of the magnetite (C) and a crystal of 715 nm (D).

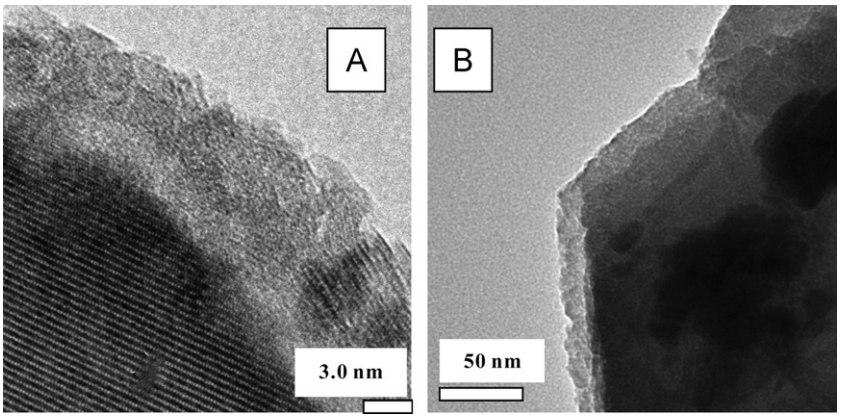

Fig. 7. The amorphous oxide corona of magnetite crystals from BIF (A) and biogenic magnetite after high P–T treatment (B).

would have been available for subsequent metamorphism (Nealson and Myers, 1990; Konhauser et al., 2005).

The detection of Fe(III)-organic bonds in both BIF-magnetite and biogenic magnetite of modern DIR cultures (Li et al., 2011a) certainly supports this hypothesis. Indeed, DIR mineral assemblages have shown that the assemblages of ferrihydrite + magnetite + ferrocarbonate + Fe(III)-salt of acetate can be transformed into hematite + magnetite + ferrocarbonate + Fe(III)-salt of acetate assemblage in BIF (Posth et al., 2008; Koehler et al., 2010; Li et al., 2011a). Interestingly, the organic carbon co-precipitated with iron, as estimated by Trendall (2002), was comparable to the ratio of ferrihydrite to carbon substrate left at the end of the DIR incubations in regular culturing experiments (e.g., Roh et al., 2003; Roden, 2003).

5. Conclusions

Our experimental findings suggest that bacteria played a crucial role in BIF magnetite formation, from the initial precipitation of BIF precursor minerals (e.g., poorly crystalline ferric oxyhydroxides such as ferrihydrite) to the diagenetic formation of magnetite via DIR to the metamorphic enlargement of that magnetite due to the consumption of residual organic materials derived from cell biomass. Our results further provide an explanation for the coarsening mechanism of the "primary" submicrometer to micrometer-sized biogenic magnetite into the larger, several tens of µm magnetite widely observed in banded iron formation.

Acknowledgment

We thank Professor Axel Hofmann of the University of Johannesburg for providing the Kuruman BIF samples. YLL was financially supported by General Research Funding (HKU703609P) from the Research Grants Council of Hong Kong. KOK was supported by the Natural Sciences and Engineering Research Council of Canada (NSERC), while AK was supported by research grants (KA 1736/4-1 and KA 1736/12-1) from the German Research Foundation (DFG).

References

Ayres, D.E., 1972. Genesis of iron-bearing minerals in banded iron formation mesobands in the Dales Gorge Member, Hamersley Group, Western Australia. Econ. Geol. 67, 1214–1233.

Banfield, J.F., Welch, S.A., Zhang, H.Z., Ebert, T.T., Penn, R.L., 2000. Aggregation-based crystal growth and microstructure development in natural iron oxyhydroxide biomineralization products. Science 289, 751–754.
Bazylinski, D.A., Frankel, R.B., Konhauser, K.O., 2007. Modes of biomineralization of magnetite by microbes. Geomicrobiol. J. 24, 465–475.
Bekker, A., Slack, F.J., Planavsky, N., Krapež, B., Hofmann, A., Konhauser, K.O., Rouxel, O.J., 2010. Iron formation: the sedimentary product of a complex interplay among mantle, tectonic, oceanic and biospheric processes. Econ. Geol. 105, 467–508.
Blank, C.E., Sánchez-Baracaldo, P., 2010. Timing of morphological and ecological innovations in the cyanobacteria—a key to understanding the rise in atmospheric oxygen. Geobiology 8, 1–23.
Chang, S.-S.R., Kirschvink, J.L., 1989. Magnetofossils, the magnetization of sediments, and the evolution of magnetite biomineralization. Annu. Rev. Earth Planet. Sci. 17, 169–195.
Cloud, P., 1965. Significance of the Gunflint (Precambrian) microflora photosynthetic oxygen may have had important local effects before becoming a major atmospheric gas. Science 148, 27–35.
Cloud, P., 1973. Paleoecological significance of the banded iron formation. Econ. Geol. 68, 1135–1143.
Cornell, R.M., Schwertmann, U., 1996. The Iron Oxides. VCH, Weinheim, p. 573.
Dimroth, E., 1976. Aspects of the sedimentary petrology of cherty iron formation. In: Wolf, K.H. (Ed.), Handbook of Strata-Bound and Stratiform Ore Deposits, 7. Elsevier, Amsterdam, pp. 157–201.
Ewers, W.E., Morris, R.C., 1981. Studies of the Dales Gorge Member of the Brockman iron formation, Western Australia. Econ. Geol. 76, 1929–1953.
Floran, R.J., Papike, J.J., 1975. Petrology of the low-grade rocks of the Gunflint iron-formation, Ontario–Minnesota. Geol. Soc. Am. Bull. 86, 1169–1190.
Fralick, P., Pufahl, P.K., 2006. Iron formation in Neoarchean Deltaic Successions and the microbially mediated deposition of transgressive systems tracts. J. Sediment. Res. 76, 1057–1066.
Frankel, R.B., Bazylinski, D.A., 2003. Biologically induced mineralization by bacteria. Rev. Mineral. Geochem. 54, 95–114.
Fredrickson, J.K., Zachara, J.M., Kennedy, D.W., Dong, H., Onstott, T.C., Hinman, N.W., Li, S.M., 1998. Biogenic iron mineralization accompanying the dissimilatory reduction of hydrous ferric oxide by a groundwater bacterium. Geochim. Cosmochim. Acta. 62, 3239–3257.
French, B.M., 1968. Progressive contact metamorphism of the Biwabik iron-formation, Mesabi Range, Minnesota. Minn. Geol. Surv. Bull. 45, 103.
Frost, C.D., von Blanckenburg, F., Schoenberg, R., Frost, B.R., Swapp, S.M., 2007. Preservation of Fe isotope heterogeneities during diagenesis and metamorphism of banded iron formation. Contrib. Mineral. Petrol. 153, 211–235.
Golden, D.C., Ming, D.W., Morris, R.V., Brearley, A.J., Lauer Jr., H.V., Treiman, A.H., Zolensky, M.E., Schwandt, C.S., Lofgren, G.E., McKay, G.A., 2004. Evidence for exclusively inorganic formation of magnetite in Martian meteorite ALH84001. Amer. Mineral. 89, 681–695.
Gole, M.J., 1980. Mineralogy and petrology of very-low-metamorphic grade Archaean banded iron-formations, Weld Range, Western Australia. Amer. Mineral. 65, 8–25.
Gole, M.J., Klein, G., 1981. Banded iron-formations through much of Precambrian time. J. Geol. 89, 169–183.
Hanzlik, M., Petersen, N., Keller, R., Schmidbauer, E., 1996. Electron microscopy and ^{57}Fe Mössbauer spectra of 10 nm particles, intermediate in composition between Fe_3O_4 and γ-Fe_2O_3, produced by bacteria. Geophys. Res. Lett. 23, 479–482.
Hartman, H., 1984. The evolution of photosynthesis and microbial mats: a speculation on the banded iron formations. In: Cohen, Y., Castenholz, R.W., Halvorson, H.O. (Eds.), Microbial Mats: Stromatolites. Alan R. Liss, Inc., New York, pp. 449–453.
Hegler, G., Posth, N.R., Jiang, J., Kappler, A., 2008. Physiology of phototrophic iron(II)-oxidizing bacteria: implications for modern and ancient environments. FEMS Microbiol. Ecol. 66, 250–260.
Holm, N.G., 1989. The $^{13}C/^{12}C$ ratios of siderite and organic matter of a modern metallifoerous hydrothermal sediment and their implications for banded iron formations. Chem. Geol. 77, 41–45.
Johnson, C.M., Beard, B.L., Beukes, N.J., Klein, C., O'Leary, J.M., 2003. Ancient geochemical cycling in the Earth as inferred from Fe isotope study of banded iron formations from the Transvaal Craton. Contrib. Mineral. Petrol. 144, 523–547.
Johnson, C.M., Roden, E.E., Welch, S.A., Beard, B.L., 2005. Experimental constrains on Fe isotope fractionation during magnetite and Fe carbonate formation coupled to dissimilatory hydrous ferric oxide reduction. Geochim. Cosmochim. Acta 69, 963–993.
Kallay, N., Žalac, S., 2002. Stability of nanodispersions: a model for kinetics of aggregation of nanoparticles. J. Colloid Interface Sci. 253, 70–76.
Kappler, A., Pasquero, C., Konhauser, K.O., Newman, D.K., 2005. Deposition of banded iron formations by anoxygenic phototrophic Fe(II)-oxidizing bacteria. Geology 33, 865–868.
Kaufman, A.J., 1996. Geochemical and mineralogical effects of contact metamorphism on banded iron-formation: an example from the Transvaal Basin, South Africa. Precambrian Res. 79, 171–194.
Kashefi, K., Lovley, D.R., 2003. Extending the upper temperature limit for life. Science 301, 934.
Klein, C., 2005. Some Precambrian banded iron-formations (BIFs) from around the world: their age, geological setting, mineralogy, metamorphism, geochemistry, and origins. Amer. Mineral. 90, 1473–1499.
Klein Jr., C., 1974. Greenlite, stilpnomelane, minnesotaite, crocidolite, and carbonates in a very low-grade metamorphic Precambrian iron-formation. Can. Mineral. 12, 475–498.
Klein, C., Beukes, N.J., 1992. Time distribution, stratigraphy, sedimentologic setting, and geochemistry of Precambrian iron-formations. In: Schopf, J.W., Klein, C. (Eds.), The Proterozoic Biosphere: a Multidisciplinary Study. Cambridge University Press, pp. 139–146.
Klein Jr., C., Fink, R.P., 1976. Petrology of the Sokoman Iron formation in the Howells River area, at the western edge of the Labrador trough. Econ. Geol. 71, 453–487.
Koehler, I., Konhauser, K., Kappler, A., 2010. Role of microorganisms in banded iron formations. In: Barton, L.L., et al. (Eds.), Geomicrobiology: Molecular and Environmental Perspective. Springer Science+Business Media B.V, pp. 309–324, http://dx.doi.org/10.1007/978-90-481-9204-5_14.
Konhauser, K.O., Hamade, T., Raiswell, R., Morris, R.C., Ferris, F.G., Southam, G., Canfield, D.E., 2002. Could bacteria have formed the Precambrian banded iron formations? Geology 30, 1079–1082.
Konhauser, K.O., Newman, D.K., Kappler, A., 2005. The potential significance of microbial Fe(III) reduction during deposition of Precambrian banded iron formations. Geobiology 3, 167–177.
Konhauser, K.O., Kappler, A., Roden, E.E., 2011. Iron in microbial metabolisms. Elements 7, 89–93.
Krapež, B., Barley, M.E., Pickard, A.L., 2003. Hydrothermal and resedimented organics of the precursor sediment to banded iron formation: sedimentalogical evidence from the early Paleoproterozoic Brockman Supersequence of Western Australia. Sedimentology 50, 979–1011.
La Berge, G.L., 1964. Development of magnetite in iron-formations of the Lake Superior region. Econ. Geol. 59, 1313–1342.
Li, Y.L., Konhauser, K.O., Cole, D.R., Phelps, T.J., 2011a. Mineral ecophysiological evidences of microbial activity in 2480 million years old banded iron formation. Geology 39, 707–710.
Li, Y.L., Deng, K., Zhu, S.Y., 2011b. Mössbauer hyperfine parameters of iron species in the course of Geobacter-mediated magnetite mineralization. Phys. Chem. Miner. 38, 701–708.
Li, Y.L., Pfiffner, S.M., Dyar, M.D., Konhauser, K., Vali, H., Cole, D.R., Phelps, T.J., 2009. Degeneration of biogenic superparamagnetic magnetite. Geobiology 7, 25–34.
Liu, S.V., Zhou, J., Zhang, C., Cole, D.R., Gajdarziska-Josifovska, M., Phelps, T.J., 1997. Thermophilic Fe(III)-reducing bacteria from the deep subsurface: the evolutionary implications. Science 277, 1106–1109.
Marqusee, J.A., Ross, J., 1984. Theory of Ostwald ripening: competitive growth and its dependence on volume fraction. J. Chem. Phys. 80, 536–543.
Miyano, T., Klein, C., 1983. Conditions of riebeckite formation in the iron-formation of the Dales Gorge Member, Hamersley Group, Western Australia. Amer. Mineral. 68, 517–529.
Nealson, K.H., Myers, C.R., 1990. Iron reduction by bacteria: a potential role in the genesis of banded iron formation. Amer. J. Sci. 290-A, 35–45.
Nesbit, E.G., Sleep, N.H., 2001. The habitat and nature of early life. Nature 409, 1083–1091.
Pecoits, E., Gingras, M.K., Kappler, A., Posth, N.R., Barley, M.A., Konhauser, K.O., 2009. Petrography and trace element geochemistry of Dales Gorge banded iron formation: paragenetic sequence, source and implications for palaeo-ocean chemistry. Precambrian Res. 172, 163–187.
Perez-Gonzalez, T., Jimenez-Lopez, G., Neal, A.L., Rull-Perez, F., Rodriguez-Navarro, A., Fernandez-Vivas, A., Ianez-Pareja, E., 2010. Magnetite biomineralization induced by *Shewanella oneidensis*. Geochim. Cosmochim. Acta 74, 967–979.
Pickard, A.L., 2003. SHRIMP U-Pb zircon ages for the Palaeoproterozoic Kuruman Iron Formation, Northern Cape Province, South Africa: evidence for simultaneous BIF deposition on Kaapvaal and Pilbara Cratons. Precambrian Res. 125, 275–315.
Piepenbrock, A., Dippon, U., Porsch, K., Appel, E., Kappler, A., 2011. Dependence of microbial magnetite formation on humic substance and ferrihydrite concentrations and Fe(II):Fe(total) ratio. Geochim. Cosmochim. Acta 75, 6844–6858.
Posth, N.R., Hegler, F., Konhauser, K.O., Kappler, A., 2008. Alternating Si and Fe deposition caused by temperature fluctuations in Precambrian oceans. Nat. Geosci. 1, 703–708.
Posth, N.R., Huelin, S., Konhauser, K.O., Kappler, A., 2010. Size, density and mineralogy of cell-mineral aggregates formed during anoxygenic phototrophic Fe(II) oxidation. Geochim. Cosmochim. Acta 74, 3476–3493.
Roden, E.E., 2003. Fe(III) oxide reactivity toward biological versus chemical reduction. Environ. Sci. Technol. 37, 1319–1324.
Roh, Y., Zhang, C.-L., Vali, H., Lauf, R.J., Zhou, J., Phelps, T.J., 2003. Biogeochemical and environmental factors in Fe biomineralization: magnetite and siderite formation. Clays Clay Miner. 51, 83–95.
Schädler, S., Burkhardt, C., Hegler, F., Straub, K.L., Miot, J., Benzerara, K., Kappler, A., 2009. Formation of cell-iron-mineral aggregates by phototrophic and nitrate-reducing anaerobic Fe(II)-oxidizing bacteria. Geomicrobiol. J. 26, 93–103.
Sparks, N.H.C., Mann, S., Bazylinski, D.A., Lovley, D.R., Jannasch, H.W., Frankel, R.B., 1990. Structure and morphology of magnetite anaerobically-produced by a marine magnetotactic bacterium and a dissimilatory iron-reducing bacterium. Earth Planet. Sci. Lett. 98, 14–22.
Steinhoefel, G., Horn, I., von Blanckenburg, F., 2009. Micro-scale tracing of Fe and Si isotope signatures in banded iron formation using femtosecond laser ablation. Geochim. Cosmochim. Acta 73, 5343–5360.
Thomas-Keprta, K.L., Bazylinski, D.A., Kirschvink, J.L., Clemett, S.J., McKay, D.S., Wentworth, S.J., Vali, H., Gibson, E.K., Romanek, C.S., 2000. Elongated prismatic magnetite crystals in ALH84001 carbonate globules: potential Martian magnetofossils. Geochim. Cosmochim. Acta 64, 4049–4081.
Thomas-Keprta, K.L., Clemett, S.J., McKay, D.S., Gibson, E.K., Wentworth, S.J., 2009. Origins of magnetite nanocrystals in Martian meteorite ALH84001. Geochim. Cosmochim. Acta 73, 6631–6677.

Trendall, A.F., 2002. The significance of iron-formation in the Precambrian stratigraphic record. In: Altermann, W., Corcoran, P.L. (Eds.), Precambrian Sedimentary Environments: A Modern Approach to Depositional Systems, 33. Special Publications of the International Association of Sedimentology, pp. 33–66.

Vargas, M., Kashefi, K., Blunt-Harris, E.L., Lovley, D.R., 1998. Microbiological evidence for Fe(III) reduction on early Earth. Nature 395, 65–67.

Viswanathiah, M.N., Tareen, J.A.K., Krishnamusthy, K.V., 1980. Low temperature hydrothermal synthesis of magnetite. J. Cryst. Growth 49, 189–192.

Yamaguchi, K.E., Johnson, C.M., Beard, B.L., Ohomoto, H., 2005. Biogeochemical cycling of iron in the Archean–Palaeoproterozoic Earth: constrains from iron isotope variations in sedimentary rocks from the Kaapvaal and Pilbara Cratons. Chem. Geol. 218, 135–169.

Zhang, C.L., Vali, H., Romanek, C.S., Phelps, T.J., Liu, S.V., 1998. Formation of single-domain magnetite by a thermophilic bacterium. Am. Mineral. 83, 1409–1418.

Zegeye, A., Mustin, C., Jorand, F., 2010. Bacterial and iron oxide aggregates mediate secondary mineral formation: green rust versus magnetite. Geobiology 8, 209–222.